REPORT ON 3D MAGNETIC FIELD SIMULATIONS

In this report, results of 3D magnetic field simulations by FEMLAB and input parameters for the final version of the design are reported. Theoretical foundations of the simulations, with special emphasis of Nd-Fe-B magnets modeling, are briefly presented in the first part of the report.

Krzysztof Turek

Year 2005

1. Methods of Problems Solving in Magnetostatics

The basic equations in magnetostatic are:

$$\vec{\nabla} \cdot \vec{B} = 0 \qquad \text{and} \qquad \vec{\nabla} x \vec{H} = \vec{j} \,. \tag{1}$$

Additional equations relate the magnetic flux density $\vec{B}$ and the field strength $\vec{H}$ in the problem subdomains. The relationships depend on the subdomain material. In vacuum $\vec{B}$ is parallel to $\vec{H}$ and proportional in magnitude.

$$\vec{B} = \mu_0 \vec{H} \,, \tag{2}$$

where $\mu_0 = 4\pi 10^{-7}$ is the vacuum magnetic permeability. In ferromagnetic materials $\vec{B}$ is the non linear function of $\vec{H}$ that depends on the material, the problem geometry, and the material magnetic history. This dependency on the variety of parameters is the main obstacle in solving problems in magnetostatic.

Ideal soft ferromagnetic materials are considered to have not histeresis and the magnetic flux density $\vec{B}$ is then also parallel to $\vec{H}$ but generally not proportional in magnitude. The relationship between $\vec{B}$ and $\vec{H}$ can be usually accepted as linear in virgin, soft ferromagnetic materials in weak applied magnetic field strength and the proportionality constant is,

$$\vec{B} = \mu \vec{H} \,, \tag{3}$$

where μ is the magnetic permeability of material. The permeability μ is related to μ_0 through the relative permeability μ_r,

$$\mu = \mu_0 \mu_r \,. \tag{4}$$

In hard magnetic materials $\vec{B}$ and $\vec{H}$ are generally not parallel because of material contribution to the flux density throughout magnetization vector $\vec{M}$ that resists to changes in magnitude and direction by coercivity mechanism. Consequently it is convenient to represent the material contribution separately from the free space component,

$$\vec{B} = \mu_0 \left(\vec{H} + \vec{M} \right), \tag{5}$$

where B is in the units of tesla (T) or webers per square meter (Wb/m^2), H and M are in ampers per metr (A/m) and μ_0 in henry per meter (H/m). The equation (5) for flux density is written in either of four ways,

$$\vec{B} = \mu_0 \vec{H} + \vec{B}_i \qquad \text{or} \qquad \vec{B} = \mu_0 \vec{H} + \vec{J} \tag{6a}$$

$$\vec{B} = \vec{B}_0 + \vec{B}_i \qquad \text{or} \qquad \vec{B} = \vec{B}_0 + \vec{J} \tag{6b}$$

The material property carried by $\vec{B}_i$ or $\vec{J}$ is called 'intrinsic induction", "intrinsic flux density", or 'magnetic polarization". The relationship between magnetic flux density, field intensity and magnetization as in (6b) has the advantage that all three quantities involved are of the same kind and are measured in teslas. In the ideal linear materials *M* is related to *H* throughout magnetic susceptibility χ,

$$M = \chi H \qquad (7)$$

The substitution of (7) to (5) gives,

$$\vec{B} = \mu_0(1+\chi)\vec{H}\,. \qquad (8)$$

It follows from the comparison of (8) with (3) and (4) that magnetic susceptibility differs of 1 from relative magnetic permeability,

$$\mu_r = 1+\chi \qquad (9)$$

Magnetic field may be produced either by ferromagnetic materials or by electric currents. If like in the Nd-Fe-B magnet for MRI scanner the magnetic field is produced only by permanent magnets, the current density in the problem volume is equal to 0 and consequently rotation of field intensity in (1) vanishes. For the problems of that kind we can introduce magnetic scalar potential V_m,

$$\vec{H} = -\nabla V_m\,. \qquad (10)$$

The relationship (7) is not valid for premagnetized materials (permanent magnets), but still magnetization can be related to the field intensity by linear expression,

$$\vec{M} = \vec{M}_0 + \chi\vec{H} = \vec{M}_0 + (\mu_r - 1)\vec{H}\ , \qquad (11)$$

where $\vec{M}_0$ is premagnetization of the magnet. Substituting the right side of (11) for $\vec{M}$ in **(5)** we obtain,

$$\vec{B} = \mu_0\mu_r\vec{H} + \mu_0\vec{M}_0 \qquad (12)$$

Combining (12) together with the first equation (1) we can derive an equation for magnetostatic potential,

$$-\nabla\cdot(\mu_0\mu_r\nabla V_m - \mu_0 M_0) = 0\,. \qquad (13)$$

All simulations described in this report were based on this equation.

2. Permanent magnets

Within magnetic material magnetic field strength $\vec{H}$ is determined by divergence of polarization that negative is called magnetic pole or charge density ρ_m by analogy to the electrical charge density,

$$\rho_m = -\vec{\nabla} \cdot \vec{J} . \qquad (14)$$

Continuing the analogy, an incremental magnetic charge can be related to volume charge distribution,

$$dq_m = \rho_m dv \qquad (15)$$

or to the a surface charge distribution,

$$dq_m = \vec{J} \cdot d\vec{s} . \qquad (16)$$

The incremental magnetic charge located $\vec{r}_1$ contributes to the magnetic field $\vec{H}$ at a location $\vec{r}_2$ with an increment $d\vec{H}$ defined by the magnetostatic Coulomb law,

$$d\vec{H}(\vec{r}_2) = \frac{\vec{r} dq_m}{4\pi\mu_0 r^3}, \qquad (17)$$

where $\vec{r} = \vec{r}_2 - \vec{r}_1$

$\vec{H}$ is the integral of Eq. (17) over all magnetic charges. To map the field the integration must be repeated for each point of the mapped region. This procedure, though conceptually very simple is a formidable problem in practice since generally magnetic charge distribution is not known. Consequently complex numerical methods are developed to make the procedure useful for solving magnetostatic problems. The problem extremely simplifies if the magnetic region has a simple geometry and is homogeneously polarized like an ideal cylindrical permanent magnet homogeneously polarized along its symmetry axis. The divergence of $\vec{J}$ vanishes then in the magnet volume and magnetic field is produced only by the surface charge (16) homogeneously distributed at the pole magnet surfaces. The results of numerical integration of (17) postprocessed to the $\vec{H}$ field lines image are presented in Fig. 1.

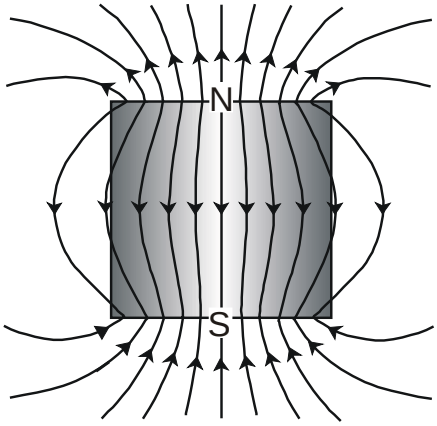

Fig. 1. *H* field produced by a cylindrical magnet homogeneously magnetized parallel to its axis.

The *H* filed lines distribution can be easy understood if to notice that due to vanishing of the volume charge density the ideal permanent magnet can be replaced with two opposite churched discs like these shown in Fig. 2. It should be remembered that the concept of magnetic charge is a useful fiction, since magnetic field is sourceless. It is apparent that the filed outside the disks planes must be opposite too that between the planes in such configuration. The H-field produced by magnet within its own volume is called demagnetization field H_d since it tries to reduce $\vec{J}$.

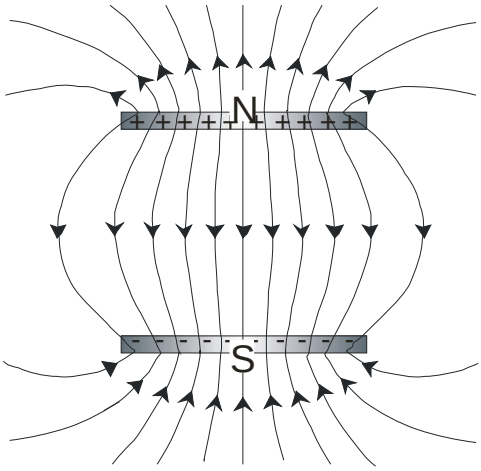

Fig. 2. An ideal cylindrical magnet from **Fig. 1**. can be replaced with two opposite charged discs.

$\vec{B}$ field can be derived from $\vec{H}$ field by (6a). The result is in Fig. 3

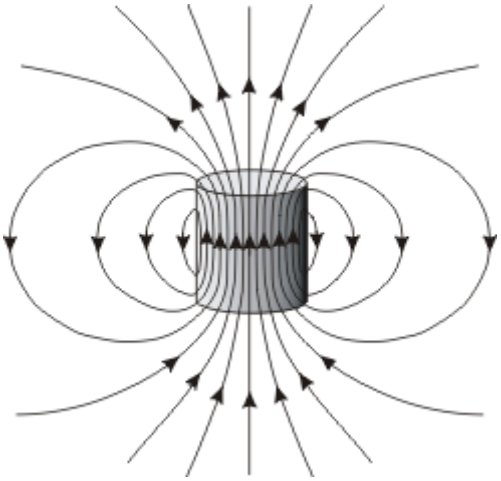

Fig. 3. The calculated B field of ideal cylindrical magnet.

Eq. (17) can be easy integrated for the observation points on the magnet axis[1]. Let the magnet of length 2h and radius r has the symmetry center at the center of coordinate s and the symmetry axis directed along z axis, as it is shown in Fig. 4.

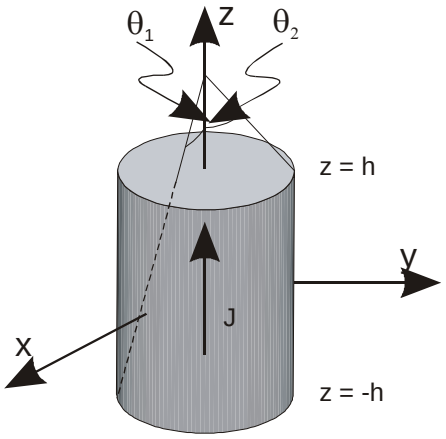

Fig. 4. Homogenously polarized magnet located at the centre of coordinate system.

Two equations are the result of integration one of which describes *H* outside the magnet and the second inside it,

$$\vec{H}(z) = \frac{\vec{J}}{2\mu_0}\left(\cos\theta_1 - \cos\theta_2\right) \quad \text{for} \quad |z| > h, \qquad (18\ a)$$

$$\vec{H}(z) = \frac{\vec{J}}{2\mu_0}\left(\cos\theta_1 - \cos\theta_2 - 2\right) \text{ for } \quad |z| < h\,, \tag{18 b}$$

where

$$\cos\theta_1 = \frac{z+h}{\sqrt{\left[(z+h)^2 + r^2\right]}} \tag{19a}$$

and

$$\cos\theta_2 = \frac{z-h}{\sqrt{\left[(z-h)^2 + r^2\right]}}\,. \tag{19b}$$

The substitution of right side of (18 a) as well (18 a) for $\vec{H}$ in (6a) gives the same equation for the flux density both in and outside the magnet,

$$\vec{B}(z) = \frac{\vec{J}}{2\mu_0}\left(\cos\theta_1 - \cos\theta_2\right), \tag{20}$$

in accordance with the general B_z component continuity condition at the boundary. Eq. (20) solved for $\vec{J}$ gives,

$$\vec{J} = \frac{\vec{B}(z)}{1 + \frac{1}{2}\left(\cos\theta_1 - \cos\theta_2 - 2\right)}\,. \tag{21}$$

It is convenient to relate both z and h in Eqs. (19a) to the magnet diameter D by the replacement of z with $z' = \frac{z}{D}$ and r with the aspect ratio $k = \frac{L}{D}$, where $L = 2h$ is the magnet length and D is the magnet diameter. This substitution makes solutions of the magnetostatic equations depend only on the relative spatial dimensions of the problem geometry. The cosines equations transforms then to:

$$\cos\theta_1 = \frac{z' + \frac{k}{2}}{\sqrt{\left[(z' + \frac{k}{2})^2 + \frac{1}{4}\right]}}, \tag{22 a}$$

$$\cos\theta_2 = \frac{z' - \frac{k}{2}}{\sqrt{\left[(z' - \frac{k}{2})^2 + \frac{1}{4}\right]}}. \qquad (22b)$$

At the magnets surface S_{+h} crossing z' axis at $z' = \frac{k}{2}$,

$$\cos\theta_{1h^+} = \frac{k}{\sqrt{\left[k^2 + \frac{1}{4}\right]}}, \qquad (23a)$$

and

$$\cos\theta_{2h^+} = 0. \qquad (23b)$$

At the magnets surface S_{-h} crossing z' axis at $z' = -\frac{k}{2}$,

$$\cos\theta_{1h^-} = 0 \qquad (24a)$$

and

$$\cos\theta_{2h^-} = -\frac{k}{\sqrt{\left[k^2 + \frac{1}{4}\right]}}. \qquad (24 \textbf{a})$$

Let us consider two extreme cases: infinitely long and infinitely thin magnet. In the first case $k \to \pm\infty$ and it follows from (23) and (24) that $\cos\theta_{1h^+} \to 1$, $\cos\theta_{2h^+} = 0$, $\cos\theta_{1h^-} = 0$ and $\cos\theta_{2h^-} \to -1$. Substitution of these limiting values to (18a) gives,

$$\lim_{k \to \infty} \vec{H}\left(\pm\frac{k}{2}\right) = \frac{\vec{J}}{2\mu_0}, \qquad (25a)$$

for the outer faces of surfaces S_{+h} and S_{-h} and substitution to (18b) results in

$$\lim_{k \to \infty} \vec{H}\left(\pm\frac{k}{2}\right) = -\frac{\vec{J}}{2\mu_0}, \qquad (25b)$$

for the inner faces of surfaces S_{+h} and S_{-h}.

Magnetic flux density at the centre of the pole surface B_{sc} can be easy measured with a Hall probe. J is equal to B divided by the geometric factor in

the denominator of Eq. (20b) that is a function of the magnet aspect ratio *k*. Since for ideal magnet $B_r = J$ the remanence of the magnet can be determined from this simple measurement. When the aspect ratio is very high then, as it follows from (25a), $B_{sc} = B_r/2$. The comparison of experimental $B_{sc}(k)$ curve with that theoretical is given in Fig. 5.

For the infinitely thin magnets $k \to 0$, $\cos\theta_{1h^+} \to 0$, $\cos\theta_{2h^+} = 0$, $\cos\theta_{1h^-} = 0$ and $\cos\theta_{2h^-} \to 0$. Consequently (18 b) gives the following limiting values:

$$\lim_{k \to 0} \vec{H}\left(\pm \frac{k}{2} \right) = 0 \qquad \text{(26a)}$$

for the outside faces of surfaces S_{+h} and S_{-h} and

$$\lim_{k \to 0} \vec{H}\left(\pm \frac{k}{2} \right) = \frac{\vec{J}}{\mu_0} \qquad \text{(25b)}$$

for the inside faces of the surfaces.

The plots of field strength calculated from (18 **a**) for the magnets of various aspect are presented in Fig. 6 and plots of flux density in Fig. 7.

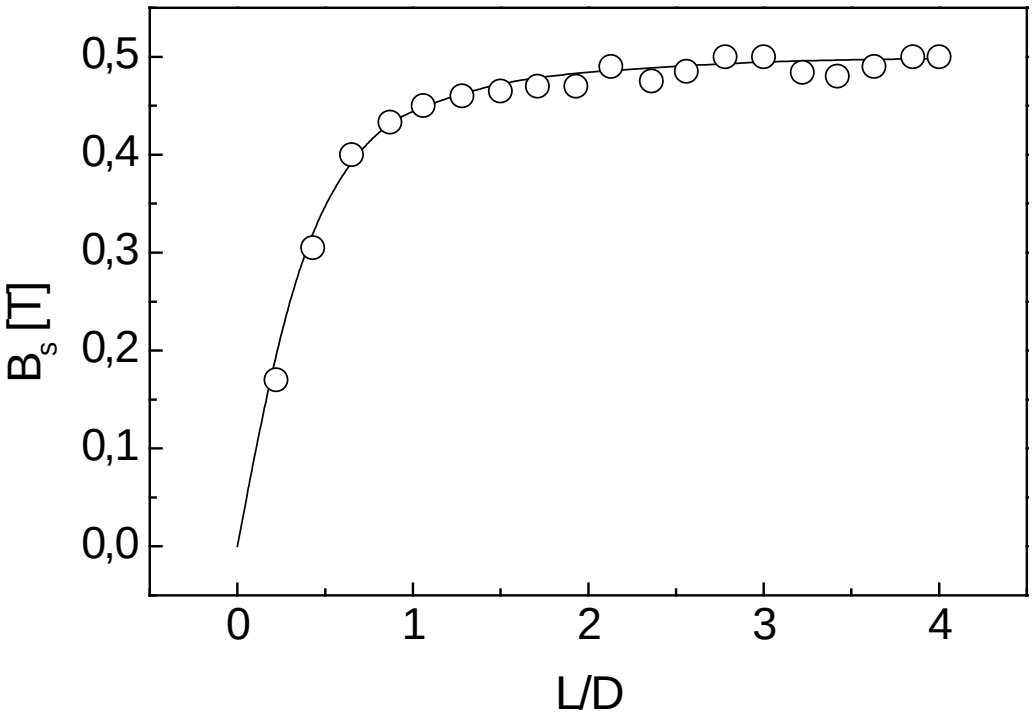

Fig. 5. Magnetic flux density at the centre of pole Nd-Fe-B cylindrical magnet versus its aspect ration $k = L/D$ (circles) and the theoretical curve $B_{sc}(k)$ (solid line).

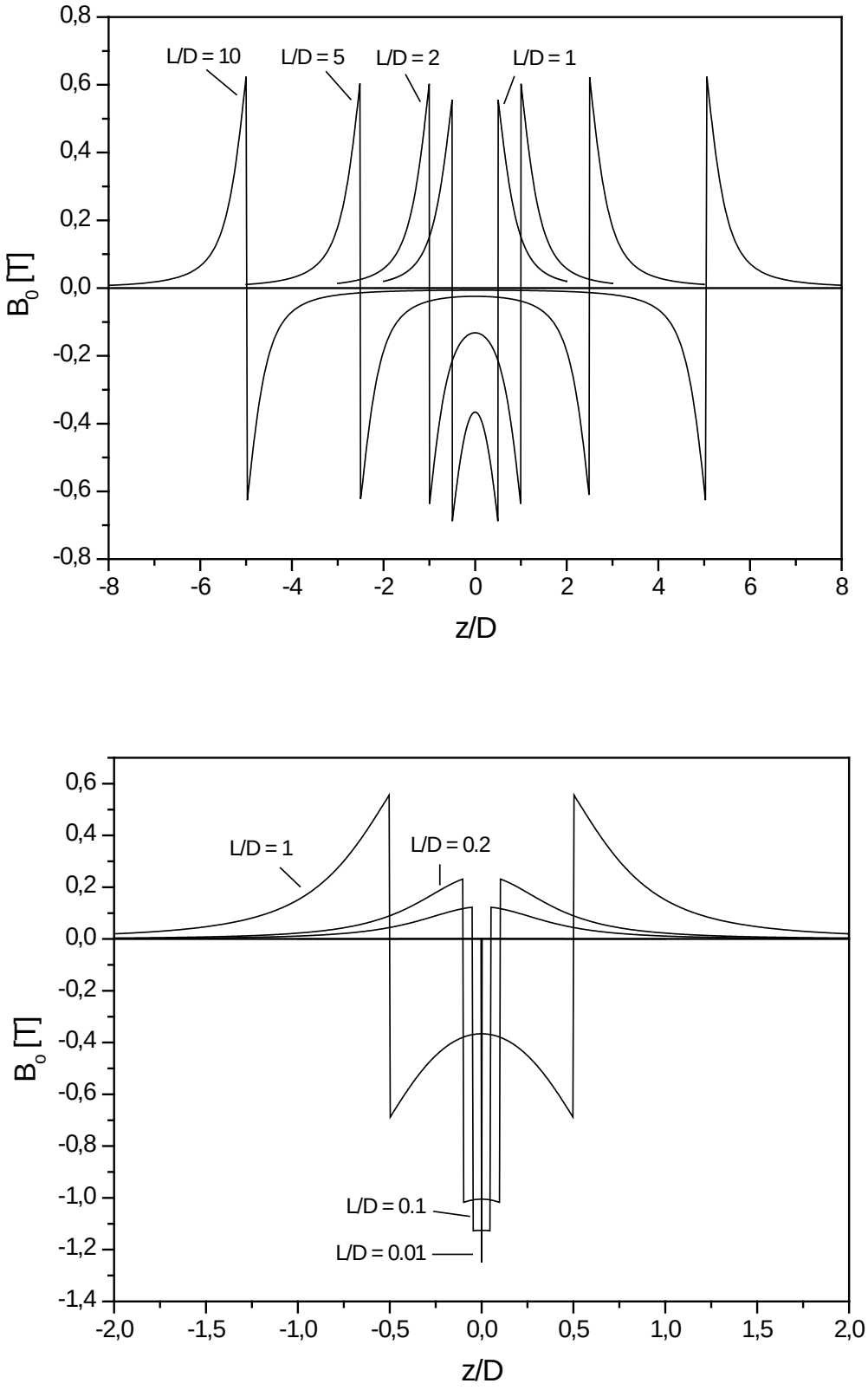

Fig. 6. Plots of the Eqs (18 a **)** for the magnets of various aspect ratio of its length L = 2h to diameter D.

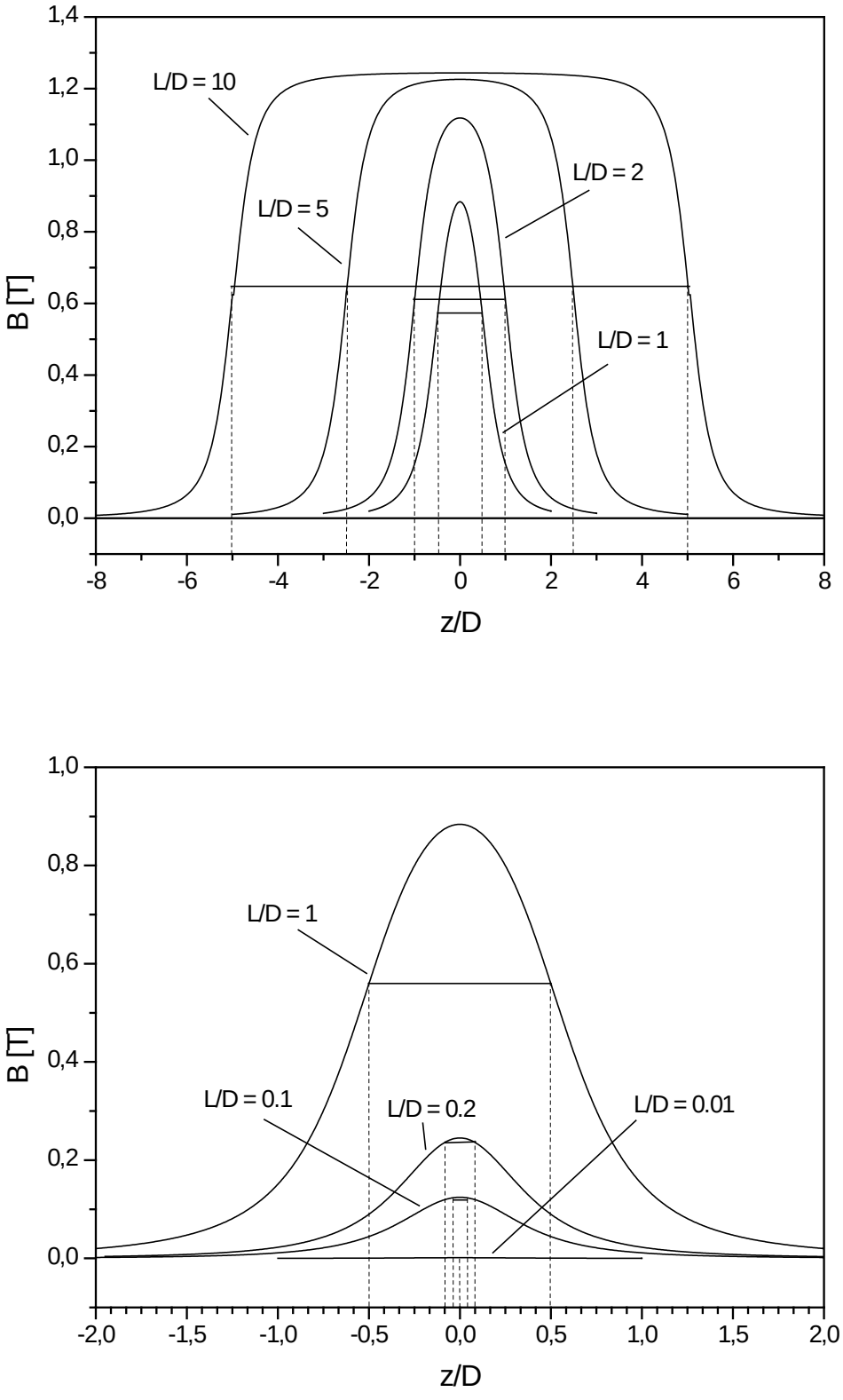

Fig. 7. Plots of the Eqs (18 a) for the magnets of various aspect ratio of its length L = 2h to diameter D.

The field produced by a magnet can be also calculated as the integral of dipole fields at a point $\vec{r}_2$ from each of magnetic moment $M(\vec{r}_1)dv$

$$d\vec{H}(\vec{r}_2) = \frac{1}{4\pi}\left(\frac{3(\vec{M}\cdot\vec{R})\vec{R}}{R^5} - \frac{\vec{M}}{R^3}\right)dv \qquad (27)$$

3. Energy considerations

Energy of the magnetic field is,

$$U = \frac{1}{2}\int \vec{B}\cdot\vec{H}dv. \qquad (28)$$

Consider a domain in empty space consisting of magnetized subdomains. The first of Eqs (1) allows to write the flux density as the rotation of vector potential $\vec{A}$,

$$\vec{B} = \nabla x\vec{A}. \qquad (29)$$

Application of vector identity

$$\nabla\cdot(\vec{A}\times\vec{H}) = (\nabla x\vec{A})\cdot\vec{H} - \vec{A}\cdot(\nabla\times\vec{H}) \qquad (30)$$

to the integral in (28) yields:

$$\int(\nabla x\vec{A})\cdot\vec{H}dv = \int\vec{A}\cdot(\nabla\times\vec{H})dv + \int\nabla\cdot(\vec{A}\times\vec{H})dv. \qquad (31)$$

The first integral at the right side of (31) is 0 since $\nabla\times\vec{H} = 0$. Using the Gauss law the second term can be written as the surface integral,

$$\int\nabla\cdot(\vec{A}\times\vec{H})dv = \iint(\vec{A}\times\vec{H})\cdot d\vec{s}. \qquad (32)$$

This integral vanishes at the boundary of infinite large sphere since $H \sim 1/r^3, A \sim 1/r^2$ and $S \sim r^2$ and consequently

$$\int\vec{B}\cdot\vec{H}dv = 0, \qquad (33)$$

when the integral is calculated over all space.

The integral (33) may be written as a sum of two integrals, one evaluated in the volume occupied by the magnet and the second in the remaining empty space; hence,

$$\int_{\text{empty space}} \vec{B} \cdot \vec{H} dv = - \int_{\text{magnet}} \vec{B} \cdot \vec{H} dv . \qquad (34)$$

The left hand side must be positive since

$$\int_{\text{empty space}} \vec{B} \cdot \vec{H} dv = \mu_0 \int_{\text{empty space}} H^2 dv \qquad (35)$$

The integral (35) is equal to twice potential energy associated with the field produced by the magnet outside its own volume.

It follows from the Eq. 4. that the potential energy can be associated with the magnet itself through the formula:

$$U = -\frac{1}{2} \int_{\text{magnet}} \vec{B} \cdot \vec{H} dv \qquad (36)$$

Since the left hand side of (34) is positive, *U* must be also positive and consequently $\vec{B}$ and $\vec{H}$ tend to be antiparallel within the magnetized domain. We came to the same conclusion considering the particular case of magnetized domain, the ideal cylindrical magnet.

The average energy density is versus aspect ratio k, calculated by FEMLAB, is plotted in Fig. 8. For the aspect ratio of 0.5 energy density reaches the maximum that is half of quantity specified in the magnets characteristics as $(BH)_{max}$.

4. Nd-Fe-B magnets

Since rare-earth permanent magnets appeared at the market of magnetic materials, a model of an ideal magnet has become closer to reality. The ideal magnet is a magnet with constant and homogenous high magnetic polarisation *J* in its whole volume, no matter how large demagnetizing field is. Thank of this property, called magnetic rigidity it is now possible to prepare uniformly magnetized blocks of any desired shape, even in the form of thin plates magnetized perpendicular to the flat surfaces, despite very high internal demagnetizing field H_d produced by such plates

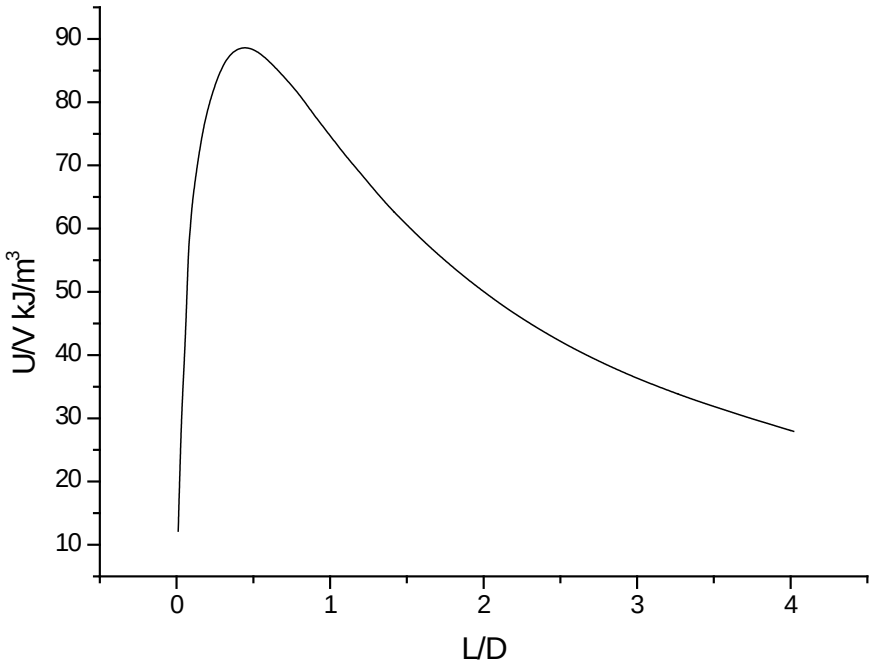

Fig. 8. Average energy density in the cylindrical magnet versus aspect ratio k = L/D.

In the previous generations of metallic permanent magnets external field usually changes the polarization in a nonlinear and irreversible way, as it is shown in

Fig. 9. The major histeresis loop is symmetric and is reproduced in each cycle of the magnetic field strength $\vec{H}$ changes, centered at $\vec{H}$ = 0, provided the amplitude of the cycle is sufficient to achieve saturation $\vec{J}_s$. If saturation is not achieved in the cycle then the curve *J(H)* takes form of minor loop totally contained within the major loop. For each of the coordinate system *J,H* and *B,H* there is a pair of characteristic points where the major histeresis loop cuts the axis: polarization remanence J_r and polarization coercivity ${}_JH_c$; induction remanence B_r and induction coercivity ${}_BH_c$. J_s is an intrinsic property of the ferromagnetic phase but both remanences J_r, B_r and coercivities ${}_JH_c$, ${}_BH_c$ depend in a complex way on the particle size, shape and metallurgical microstructure of the magnet. The *B:H* loop of Fig. 9. is related to the *J:H* loop by (6a). The ideal permanent magnets have a square hysteresis loop, $|J|=J_r$ for $|H|<{}_JH_c$, like this plotted in Fig. 10, that implies J_r to be equal to J_s. The induction coercivity in the ideal magnets with square histeresis loop and high polarization coercivity $\mu_{0J}H_c > J_r$, fulfill the condition: $\mu_{0B}H_c = J_r$. Since H_d is less than *J* and opposite in direction, coordinates J,H_d or B,H_d set points on the second quadrant of histeresis loop known as the magnet operating points. This quadrant is featured on manufacturers' data sheets, like this shown in Fig. 11.

The maximum potential energy is obtained at the point on the loop where the product $-B\cdot H$ reaches maximum and for ideal magnet,

$$\left(B \cdot H\right)_{\max} = \frac{\mu_0 B_r H_c}{4}. \qquad \textbf{(37)}$$

B_r in (37) can be replaced with J_r or J_s.

Since histeresis loop of real magnet is always included in that of ideal magnet general condition for maximum energy product is:

$$\left(B \cdot H\right)_{\max} \le \frac{\mu_0 B_r H_c}{4}. \qquad \textbf{(38)}$$

Demagnetization curves of the main four types of magnets: Nd-Fe-B, Sm-Co, Alnico and hard ferrite are shown in Fig. 12

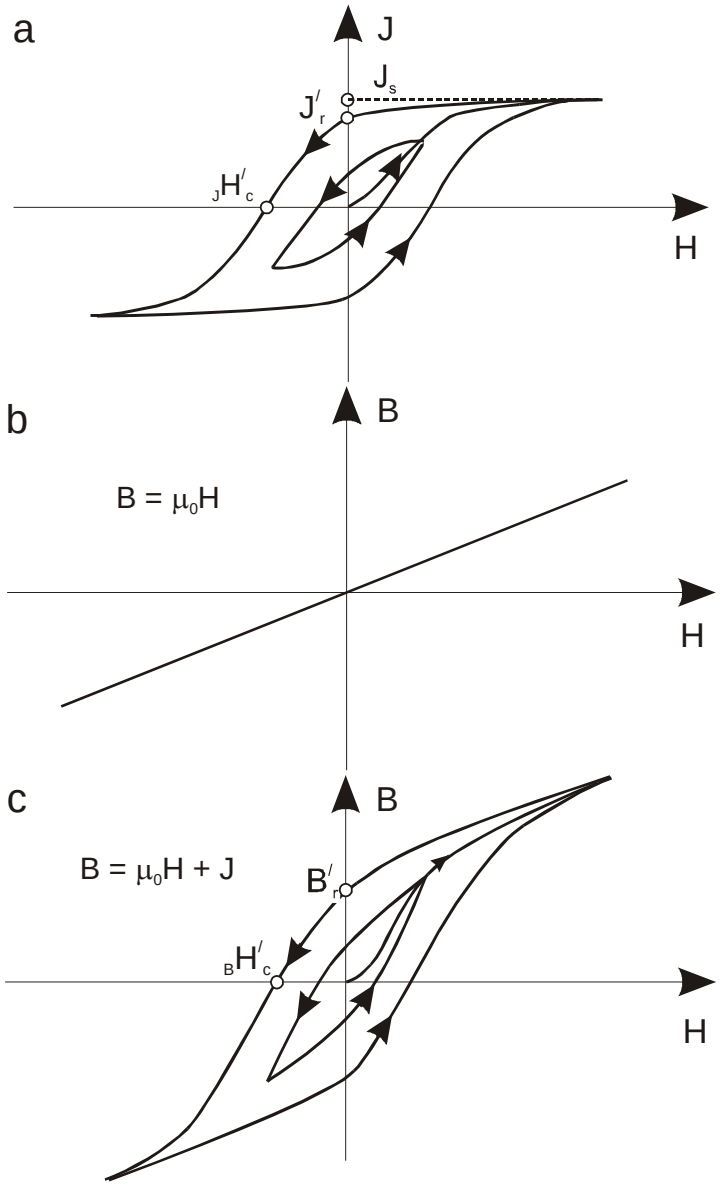

Fig. 9. The histeresis loop of magnet with the coercivity too low to keep polarization rigid.

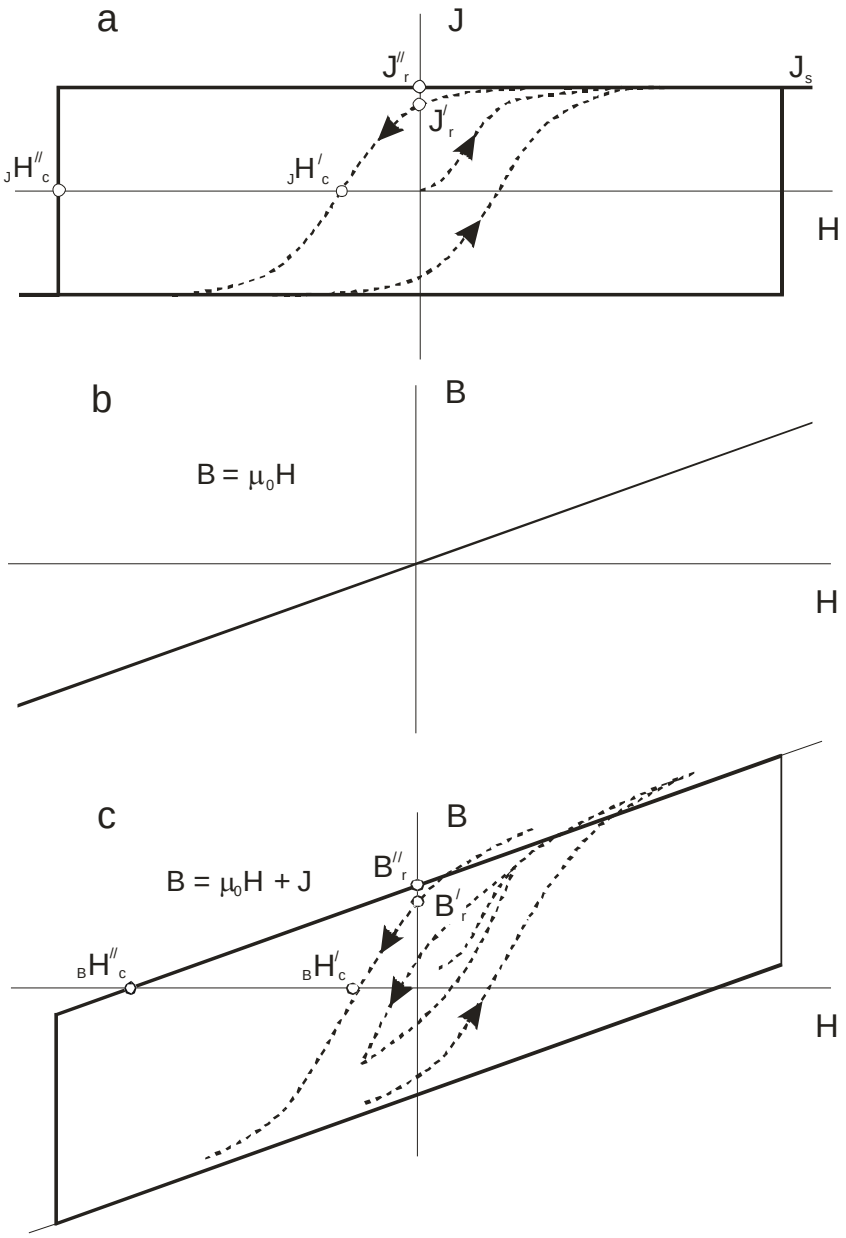

Fig. 10. The histeresis loops of ideal permanent magnet with rigid polarization (solid line) and usual magnet (dashed line).

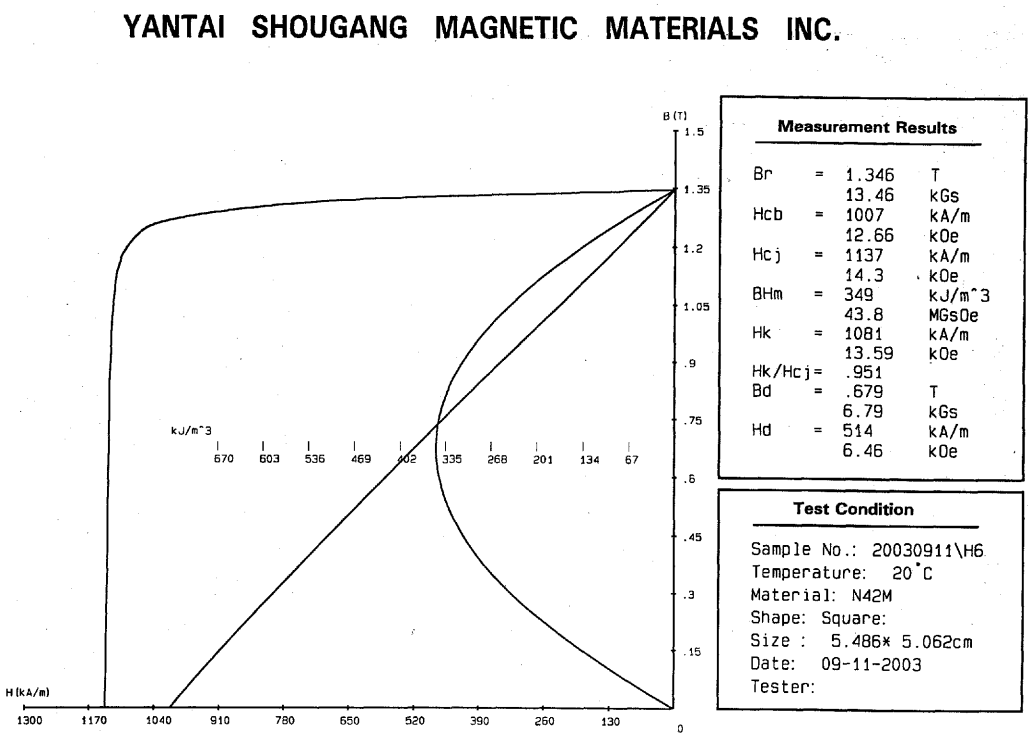

Fig. 11. Example of manufacturers' data sheet with the second quadrant of the histeresis loop.

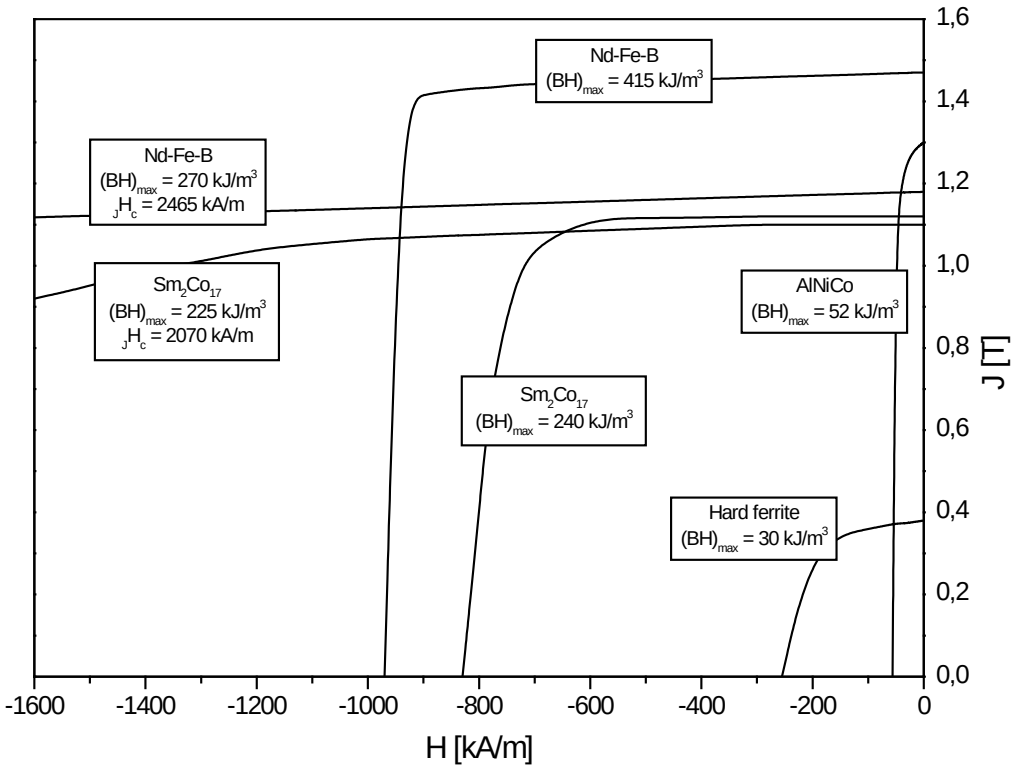

Fig. 12. Demagnetization curves for different types of magnet.

.

[1] Watson J.K., Applications of Magnetism, Jon Wiley & Sons Inc., New York, p. 96